Modulating eIF6 levels unveils the role of translation in ecdysone biosynthesis during *Drosophila* development

Arianna Russo, Guido Gatti, Roberta Alfieri, Elisa Pesce, Kelly Soanes, Sara Ricciardi, Marilena Mancino, Cristina Cheroni, Thomas Vaccari, Stefano Biffo, Piera Calamita

PII: S0012-1606(18)30796-6

DOI: https://doi.org/10.1016/j.ydbio.2019.05.013

Reference: YDBIO 8034

To appear in: *Developmental Biology*

Received Date: 5 December 2018

Revised Date: 1 May 2019

Accepted Date: 28 May 2019

Please cite this article as: Russo, A., Gatti, G., Alfieri, R., Pesce, E., Soanes, K., Ricciardi, S., Mancino, M., Cheroni, C., Vaccari, T., Biffo, S., Calamita, P., Modulating eIF6 levels unveils the role of translation in ecdysone biosynthesis during *Drosophila* development, *Developmental Biology* (2019), doi: https://doi.org/10.1016/j.ydbio.2019.05.013.

Modulating eIF6 Levels Unveils the Role of Translation in Ecdysone Biosynthesis During *Drosophila* Development

Arianna Russo[a,b], Guido Gatti[a,c], Roberta Alfieri[a,1], Elisa Pesce[a], Kelly Soanes[d], Sara Ricciardi[a,c], Marilena Mancino[a], Cristina Cheroni[a,2], Thomas Vaccari[c], Stefano Biffo[a,c]*, Piera Calamita[a,c]*

[a] INGM, National Institute of Molecular Genetics, "Romeo ed Enrica Invernizzi", via Francesco Sforza, 35 – 20122 - Milan, Italy

[b] DiSIT, Università del Piemonte Orientale, via Teresa Michel 11 -15121- Alessandria, Italy

[c] DBS, Università degli Studi di Milano, via Celoria 26 – 20133 - Milan, Italy

[d] Aquatic and Crop Resource Development - National Research Council of Canada 110, place Gymnasium Saskatoon, Saskatchewan S7N 0W9

[1] Current affiliation: Istituto di Genetica Molecolare, Centro Nazionale delle Ricerche, via Adolfo Ferrata – 27100 - Pavia, Italy

[2] Current affiliation: Istituto Europeo di Oncologia, via Adamello, 16 – 20139 - Milano, Italy

*These authors contributed equally to this work

Address correspondence to Piera Calamita or Stefano Biffo: calamita@ingm.org; biffo@ingm.org

ABSTRACT

During development, ribosome biogenesis and translation reach peak activities, due to impetuous cell proliferation. Current models predict that protein synthesis elevation is controlled by transcription factors and signalling pathways. Developmental models addressing translation factors overexpression effects are lacking. Eukaryotic Initiation Factor 6 (eIF6) is necessary for ribosome biogenesis and efficient translation. *eIF6* is a single gene, conserved from yeasts to mammals, suggesting a tight regulation need. We generated a *Drosophila melanogaster* model of eIF6 upregulation, leading to a boost in general translation and the shut-down of the ecdysone biosynthetic pathway. Indeed, translation modulation in S2 cells showed that translational rate and ecdysone biosynthesis are inversely correlated. *In vivo*, eIF6-driven alterations delayed Programmed Cell Death (PCD), resulting in aberrant phenotypes, partially rescued by ecdysone administration. Our data show that eIF6 triggers a translation program with far-reaching effects on metabolism and development, stressing the driving and central role of translation.

KEYWORDS

eIF6, ecdysone, 20HE, translation, *Drosophila* development

INTRODUCTION

During cell proliferation, ribosomal proteins (RPs) and eukaryotic Initiation Factors (eIFs) are necessary and in high demand for ribosome biogenesis and translation (1-5). Proteins involved in ribosome biogenesis do not usually have a role in the translational control and *vice versa* (6). However, the eukaryotic Initiation Factor 6 (eIF6) is remarkably unique (7): a nuclear pool is essential for nucleolar maturation of the 60S large subunit (8), while cytoplasmic eIF6 acts as a translation factor (8). Mechanistically, eIF6 is an anti-association factor: by binding 60S subunit, eIF6 prevents its premature joining with a 40S not loaded with the pre-initiation complex. Release of eIF6 is then mandatory for the formation of an active 80S (9). The dual action of eIF6 in ribosome biogenesis and translation suggests that it may act as a master gene regulating ribosomal efficiency. Remarkably, point mutations of eIF6 can revert the lethal phenotype of ribosome biogenesis factors such as SBDS (10) and eFL1p (11). eIF6 is highly conserved in yeast, fruit fly and humans (12). During evolution, the *eIF6* gene has not been subjected to gene duplication. Despite its ubiquitous role, eIF6 levels are tightly regulated *in vivo*, showing considerable variability of expression among different tissues (13). Importantly, high levels of eIF6 or hyperphosphorylated eIF6 are observed in some cancers (14, 15). eIF6 is rate limiting for tumor onset and progression in mice (16). In addition, *eIF6* amplification is observed in luminal breast cancer patients (17) and affects cancer cell metastatization (18, 19). It has been recently demonstrated that eIF6 acts at the translational level through the regulation of metabolism: in mammals, eIF6 translation activity increases fatty acid synthesis and glycolysis through the translation of transcription factors such as CEBP/β, ATF4 and CEBP/δ containing G/C rich or uORF sequences in their 5'UTR (20, 21).

However, whether eIF6 overexpression *per se* can change a transcriptional program in the absence of other genetic lesions is unknown.

Ecdysone is the primary steroid hormone in insects: during fly development, it is produced as a precursor, ecdysone (E) in the prothoracic gland (PG). Biosynthesis starts from cholesterol and, after several enzymatic steps, it is secreted in the haemolymph. Target tissues convert ecdysone into the active form, the 20-hydroxyecdysone (20HE) (22). The binding of 20HE with its receptor is responsible for a transcriptional cascade that triggers metamorphosis (23). Pulses of 20HE regulate several processes such as cell proliferation, differentiation and cell death (23-28).

To determine the effects of eIF6 high levels *in vivo*, we took advantage of *Drosophila melanogaster*, an ideal model to manipulate gene expression in a time- and tissue-dependent manner, using the GAL4/UAS system (29, 30). We reasoned that an overexpression approach could allow us to evaluate the effects of eIF6 increased activity in the context of an intact organism. To this end, we focused on the fly eye, an organ not essential for viability, whose development from epithelial primordia, the larval eye imaginal disc, is well known. The adult compound eye is a stunningly beautiful structure of approximately 800 identical units, called ommatidia (31). Each ommatidium is composed of eight neuronal photoreceptors, four glial-like cone cells and pigment cells (32, 33).

By increasing eIF6 levels specifically in the eye, we found alterations in physiological apoptosis at the pupal stage, correlating with an increase in general translation.

We observed that increased levels of eIF6 are responsible for a reshaping of the eye transcriptome that revealed a coordinated downregulation of the ecdysone

biosynthetic pathway during the larval stage. This study provides the first *in vivo* evidence that an increase in translation, dependent on heightened eIF6 levels, may drive metabolic changes and a transcriptional rewiring in a developing organ.

MATERIALS AND METHODS

Genetics

Fly strains were maintained on standard cornmeal food at 18℃. Genetic crosses were performed at 25℃, with the exception of *GMRGAL4/+* and *GMR>eIF6*, performed at 18℃. The following fly mutant stocks have been used: *GMRGAL4* was a gift from Manolis Fanto (King's College, London); *UAS-eIF6* was a gift from William J Brook (Alberta Children's Hospital, Calgary). The *eIF6* (GH08760) cDNA was obtained from the Berkeley Drosophila Genome project (Research Genetics) and sequenced for confirmation. The entire *eIF6* cDNA was cloned into the RI site of the pUAST (34). Lines obtained from the Bloomington Drosophila Stock Center (BDSC): *y[1] w[*]; P{w[+mC]=tubP-GAL4}LL7/TM3, Sb[1] Ser[1]* (5138); *spaGAL4* (26656) *P{w[+mC]=spa-GAL4.J}1, w[*]*; *54CGAL4* (27328) y*[1] w[*]; P{w[+m*]=GAL4}54C*; *w1118* (3605) *w[1118]*; *bxMS1096GAL4* (8860) w[1118] *P{w[+mW.hs]=GawB}Bx[MS1096]*.

Mosaic analysis

The *eIF6*^{k13214} mutant clones were created by *Flippase* (*FLP*) mediated mitotic recombination (35). The *eIF6*^{k13214} *(P(w[+mC]=lacW) eIF6[k13214] ytr[k13214]) P* element allele was recombined onto the right arm of chromosome two with the homologous recombination site (FRT) at 42D using standard selection techniques. Briefly, to create the FRT *y*$^{+}$ *pwn, eIF6*^{k13214} chromosomes, *eIF6*^{k13214} was recombined onto the FRT chromosome originating from the *y; P42D pwn[1] P{y+}44B/CyO* parental stock. The *yellow*$^{+}$ *pwn eIF6*^{k13214}*G418* resistant flies were selected to create stocks for clonal analysis. Similarly, stocks used for generating unmarked *eIF6*^{k13214} clones were created by recombining *eIF6*^{k13214} with the 42D FRT chromosome using the *w[1118]; P42D P{Ubi-GFP}2R/CyO* parental line.

Targeted mitotic wing clones were generated by crossing flies with *UAS-FLP*, the appropriate GAL4 driver and the suitable *42D* FRT second chromosome with the *42D* FRT *eIF6*^{k13214}. The *hs* induced *eIF6*^{k13214} mitotic clones were created by following standard techniques. Briefly, 24- and 48-hours larvae with the appropriate genotypes were heat shocked for 1 hour at 37℃ foll owed by incubation at 25℃.

S2 cell culture

The *Drosophila* S2 cells (RRID: CVCL_TZ72) were grown in Schneider medium (Lonza, Basel, Switzerland, #04-351Q) supplemented with 10% Fetal Bovine Serum (FBS – #ECS0180L, Euroclone, Pero, Italy) and 5 mL of PSG 1X (100X composition: 10000 U/mL Penicillin, 10 mg/mL Streptomycin and 200 mM L-Glutamine in citrate buffer, (#G1146, Sigma, St. Louis, MO, USA), and maintained as a semi-adherent monolayer at standard culture conditions at 25 ℃ w ithout CO_2. For protein synthesis measurement, S2 cells were treated at 65-70% confluence with 1 µM rapamycin (#R8781, Sigma) for 2 hours or 1 µM insulin (#I0516, Sigma) for 12 hours, both at 25 ℃. For SUnSET assay, the medium was removed and re placed with fresh medium supplemented with 5 µg/mL puromycin (#A1113803, Thermofisher Scientific, Waltham, MA, USA) for 3 hours, and treated according to (36).

RNA isolation and RNA sequencing

Total RNA was extracted with the mirVana^{TM} isolation kit according to the manufacturer protocol (#AM 1560, ThermoFisher) from 10 eye imaginal discs (larval stage) or 10 retinae (pupal stage). The RNA quality was controlled with BioAnalyzer (Agilent, Santa Clara, CA, USA). Libraries for Illumina sequencing were constructed from 100 ng of total RNA with the Illumina TruSeq RNA Sample Preparation Kit v2 (Set A) (Illumina, San Diego, CA, USA). The generated libraries were loaded on to the cBot (Illumina) for clustering on a HiSeq Flow Cell v3. The flow cell was then

sequenced using a HiScanSQ (Illumina). A paired-end (2×101) run was performed using the SBS Kit v3 (Illumina). Sequence deepness was at 35 million reads. For quantitative PCR, the same amount of RNA was retrotranscribed according to SuperScript™ III First-Strand Synthesis SuperMix manufacturer protocol (#18080400, LifeTechnologies, Carlsbad, CA, USA). For RNA-Seq validation, TaqMan probes specific for *eIF6* (Dm01844498_g1) and *rpl32* (Dm02151827_g1) were used, together with standard primers (*rpl32* Fwd CGGATCGATATGCTAAGCTGT, Rev CGACGCACTCYCYYGTCG; *shd* Fwd CGGGCTACTCGCTTAATGCAG, Rev AGCAGCACCACCTCCATTTC). Target mRNA quantification was performed by using ΔCt-method with *rpl32* RNA as an internal standard, performed on a StepOne Plus System (Applied Biosystems, Foster City, CA, USA).

Bioinformatic Analysis

Read pre-processing and mapping

Three biological replicates were analyzed for *GMRGAL4*/+ and *GMR>eIF6* larval eye imaginal discs and four biological replicates were analyzed for *GMRGAL4*/+ and *GMR>eIF6* pupal retinae, for a total of 14 samples. Raw reads were checked for quality by FastQC software (version 0.11.2, S., A. FastQC: a quality control tool for high-throughput sequence data. 2010; Available from: http://www.bioinformatics.babraham.ac.uk/projects/fastqc), and filtered to remove low quality calls by Trimmomatic (version 0.32) (37) using default parameters and specifying a minimum length of 50. Processed reads were then aligned to *Drosophila melanogaster* genome assembly GRCm38 (Ensembl version 79) with STAR software (version 2.4.1c) (38).

Gene expression quantification and differential expression analysis.

HTSeq-count algorithm (version 0.6.1, option -s = no, gene annotation release 79 from Ensembl) (39) was employed to produce gene counts for each sample. To estimate differential expression, the matrix of gene counts produced by HTSeq was analyzed by DESeq2 (version DESeq2_1.12.4) (40). The differential expression analysis by the DeSeq2 algorithm was performed on the entire dataset composed by both larvae and pupae samples. The two following comparisons were analyzed: *GMR>eIF6 versus GMRGAL4/+* larval eye imaginal discs (6 samples overall) and *GMR>eIF6 versus GMRGAL4/+* pupal retinae (8 samples in total). Reads counts were normalized by calculating a size factor, as implemented in DESeq2. Independent filtering procedure was then applied, setting the threshold to the 62 percentile; 10886 genes were therefore tested for differential expression. Significantly modulated genes in *GMR>eIF6* genotype were selected by considering a false discovery rate lower than 5%. Regularized logarithmic (rlog) transformed values were used for heat map representation of gene expression profiles. Analyses were performed in R version 3.3.1 (2016-06-21, Computing, T.R.F.f.S. R: A Language and Environment for Statistical Computing. Available from: http://www.R-project.org/).

Functional analysis by topGO

The Gene Ontology enrichment analysis was performed using topGO R Bioconductor package (version topGO_2.24.0). The option *nodesize = 5* is used to prune the GO hierarchy from the terms which have less than 5 annotated genes and the *annFUN.db* function is used to extract the gene-to-GO mappings from the genome-wide annotation library *org.Dm.eg.db* for *D. melanogaster*. The statistical enrichment of GO was tested using Fisher's exact test. Both the "classic" and "elim" algorithms were used.

Gene set association analysis

Gene set association analysis for larvae and pupae samples was performed by GSAA software (version 2.0) (41). Raw reads for 10886 genes identified by Entrez Gene ID were analyzed by GSAASeqSP, using gene set C5 (*Drosophila* version retrieved from http://www.go2msig.org/cgi-bin/prebuilt.cgi?taxid=7227) and specifying as permutation type 'gene set' and as gene set size filtering min 15 and max 800.

Western blotting and antibodies

Larval imaginal discs, pupal retinae and adult heads were dissected in cold Phosphate Buffer Saline (Na_2HPO_4 10 mM, KH_2PO_4 1.8 mM, NaCl 137 mM, KCl 2.7 mM, pH 7.4) (PBS) and then homogenized in lysis buffer (HEPES 20 mM, KCl 100 mM, Glycerol 5%, EDTA pH 8.0 10 mM, Triton-X 0.1%, DTT 1mM) freshly supplemented with Protease Inhibitors (Sigma, St. Louis, MO, USA, #P8340). Protein concentration was determined by BCA analysis (Pierce, Rockford, IL, USA, #23227). Equal amounts of proteins were loaded and separated on a 10% SDS-PAGE, then transferred to a PVDF membrane. Membranes were blocked in 10% Bovine Serum Albumin (BSA) in PBS-Tween (0.01%) for 30 minutes at 37℃. The following primary antibodies were used: rabbit anti-eIF6 (1:500, this study), rabbit anti-β-actin (1:4000, CST, Danvers, MA, USA, #4967; RRID: AB_330288), mouse anti-Puromycin (1:500, Merck Millipore, #MABE343; RRID: AB_2566826). To produce the anti-eIF6 antibody used in this study, a rabbit polyclonal antiserum against two epitopes on COOH-terminal peptide of eIF6 (NH2-CLSFVGMNTTATEI-COOH eIF6 203-215 aa; NH2-CATVTTKLRAALIEDMS-COOH eIF6 230-245 aa) was prepared by PrimmBiotech (Milan, Italy, Ab code: 201212-00003 GHA/12),

purified in a CNBr-Sepharose column and tested for its specificity against a mix of synthetic peptides with ELISA test. The following secondary antibodies were used: donkey anti-mouse IgG HRP (1:5000, GE Healthcare, Little Chalfont, UK, Amersham #NA931; RRID: AB_772210) and donkey anti-rabbit IgG HRP (1:5000, GE Healthcare, Amersham #NA934; RRID: 772206).

SUnSET Assay

Larval imaginal eye and wing discs were dissected in complete Schneider medium (Lonza, Basel, Switzerland) and treated *ex vivo* with puromycin (50 µg/mL) for 30 minutes at room temperature, then fixed in 3% paraformaldehyde (PFA) for 1 hour at room temperature. Immunofluorescences were then performed as described below, using a mouse anti-puromycin (1:500, Merck Millipore, Billerica, MA, USA, #MABE343, RRID: AB_2566826) as a primary antibody. Discs were then examined by confocal microscope (Leica SP5, Leica, Wetzlar, Germany) and fluorescence intensity was measured with ImageJ software.

Cell count

GMRGAL4/+ and *GMR>eIF6* pupal retinae at 40h APF were dissected, fixed, and stained with anti-Armadillo to count cells, as previously described (42). Cells contained within a hexagonal array (an imaginary hexagon that connects the centres of the surrounding six ommatidia) were counted; for different genotypes, the number of cells per hexagon was calculated by counting cells, compared with the corresponding control. Cells at the boundaries between neighbouring ommatidia count half. At least 3 hexagons (equivalent to 9 full ommatidia) were counted for each genotype, and phenotypes were analyzed. Standard Deviation (SD) and unpaired two-tailed Student t-test were used as statistical analysis.

Immunofluorescences, antibodies and TUNEL Assay

Larval imaginal discs and pupal retinae were dissected in cold PBS and fixed in 3% paraformaldehyde (PFA) for 1 hour at room temperature, then washed twice with PBS and blocked in PBTB (PBS, Triton 0.3%, 5% Normal Goat Serum and 2% Bovine Serum Albumin) for 3 hours at room temperature. Primary antibodies were diluted in PBTB solution and incubated O/N at 4℃. After three washes with PBS, tissues were incubated O/N at 4℃ with secondary antibodies and DAPI (1:1000, Molecular Probes, Eugene, OR, USA, #D3571) in PBS. After three washes with PBS, eye imaginal discs and retinae were mounted on slides with ProLong Gold (LifeTechnologies, Carlsbad, CA, USA, #P36930). The following primary antibodies were used: rabbit anti-eIF6 (1:50, this study), rat anti-ELAV (1:100, Developmental Study Hybridoma Bank DSHB, Iowa City, IA, USA, #7E8A10; RRID: AB_528218), mouse anti-CUT (1:100, DSHB, #2B10; RRID: AB_528186), mouse anti-Armadillo (1:100, DSHB, #N27A; RRID: AB_528089), mouse anti-Chaoptin (1:100, DSHB, #24B10; RRID: AB_528161), rabbit anti- Dcp-1 (1:50, CST, #9578; RRID: AB_2721060), mouse anti-Puromycin (1:500, Merck Millipore, #MABE343; RRID: AB_2566826). The following secondary antibodies were used: goat anti-rat, goat anti-mouse, goat anti-rabbit (1:500 Alexa Fluor® secondary antibodies, Molecular Probes; RRID: AB_142924; AB_143157; AB_141778). Dead cells were detected using the In Situ Cell Death Detection Kit TMR Red (Roche, Basel, Switzerland, #12156792910) as manufacturer protocol, with some optimizations. Briefly, retinae of the selected developmental stage were dissected in cold PBS and fixed with PFA 3% for 1 hour at room temperature. After three washes in PBS, retinae were permeabilized with Sodium Citrate 0.1%-Triton-X 0.1% for 2 minutes at 4℃ and then incubated overnight at 37℃ with the enzyme mix. Retinae were then rinsed three

times with PBS, incubated with DAPI to stain nuclei and mounted on slides. Discs and retinae were examined by confocal microscopy (Leica SP5) and analyzed with Volocity 6.3 software (Perkin Elmer, Waltham, MA, USA).

Semithin sections

Semithin sections were prepared as described in (43). Adult eyes were fixed in 0.1 M Sodium Phosphate Buffer, 2% glutaraldehyde, on ice for 30 min, then incubated with 2% OsO_4 in 0.1 M Sodium Phosphate Buffer for 2 hours on ice, dehydrated in ethanol (30%, 50%, 70%, 90%, and 100%) and twice in propylene oxide. Dehydrated eyes were then incubated O/N in 1:1 mix of propylene oxide and epoxy resin (Sigma, Durcupan™ ACM). Finally, eyes were embedded in pure epoxy resin and baked O/N at 70℃. The embedded eyes were cut on a Leica Ultr aCut UC6 microtome using a glass knife and images were acquired with a 100X oil lens, Nikon Upright XP61 microscope (Nikon, Tokyo, Japan).

Ecdysone treatment

For ecdysone treatment, 20-HydroxyEcdysone (20HE) (Sigma, #H5142) was dissolved in 100% ethanol to a final concentration of 5 mg/mL; third instar larvae from different genotypes (*GMRGAL4/+* and *GMR>eIF6*) were collected and placed in individual vials on fresh standard cornmeal food supplemented with 240 µg/mL 20HE. Eye phenotype was analyzed in adult flies, and images were captured with a TOUPCAM™ Digital camera. Eye images were analyzed with ImageJ software.

***In vitro* Ribosome Interaction Assay (iRIA)**

iRIA assay was performed as described in (44). Briefly, 96-well plates were coated with a cellular extract diluted in 50 µL of PBS, 0.01% Tween-20, O/N at 4℃ in a humid chamber. The coating solution was removed and unspecific sites were

blocked with 10% BSA, dissolved in PBS, 0.01% Tween-20 for 30 minutes at 37 ℃. Plates were washed with 100 µL/well with PBS-Tween. 0.5 µg of recombinant biotinylated eIF6 were resuspended in a reaction mix: 2.5 mM $MgCl_2$, 2% DMSO and PBS-0.01% Tween, to reach 50 µL of final volume/well, added to the well and incubated with coated ribosomes for 1 hour at room temperature. To remove unbound proteins, each well was washed 3 times with PBS, 0.01% Tween-20. HRP-conjugated streptavidin was diluted 1:7000 in PBS, 0.01% Tween-20 and incubated in the well, 30 minutes at room temperature, in a final volume of 50 µL. Excess of streptavidin was removed through three washes with PBS-Tween. OPD (o-phenylenediamine dihydrochloride) was used according to the manufacturer's protocol (Sigma-Aldrich) as a soluble substrate for the detection of streptavidin-peroxidase activity. The signal was detected after the incubation, plates were read at 450 nm on a multiwell plate reader (Microplate model 680, Bio-Rad, Hercules, CA, USA).

EIA assay

Ecdysone levels from eye imaginal discs and retinae were titred according to the 20HE Enzyme Immunoassay kit protocol (Bertin Pharma, Montigny le Bretonneux, France, #A05120.96). Standard curves were generated using 20HE provided by the kit. Absorbance was measured at 405 nm with Tecan Freedom EVO (Tecan, Männedorf, Switzerland).

RESULTS

Increased eIF6 levels cause embryonic lethality and aberrant morphology

Regulation of eIF6 levels is stringent in normal conditions (13), with evidence for eIF6 amplification (17) and overexpression (12, 14, 45-47) in cancer. We used the *Drosophila melanogaster* model to establish whether an increased activity of eIF6 could drive specific developmental decisions.

First, we assessed the effects caused by the loss of the *eIF6 D. melanogaster* homologue. To this end, we used the *P* element allele $eIF6^{k13214}$ (48), to induce mitotic clones homozygous for $eIF6^{k13214}$ in first instar larvae by heat shock-induced FLIP/*FLP*-mediated homologous recombination (35). We did not observe clones of eIF6 mutant cells in all adult tissues, with the exception of small ones in the wing margin (S1A Fig). Similar results were obtained in a *minute* background that provides a growth advantage to mutant cells, or by targeted expression of FLP in the wing margin (S1A Fig). Together, these results confirm that eIF6 is required for cell viability in *Drosophila*, as previously observed in yeast (15) and mammals (8), precluding significant studies on the effects of eIF6 inhibition.

Next, we assessed the effects of eIF6 high levels, by ubiquitous expression of *eIF6* under the *TubGAL4* driver. Ectopic expression resulted in late embryonic lethality (S1B Fig). To circumvent early lethality, we focused on a non-essential fly organ, the eye. Increased eIF6 expression during late larval eye disc development, driven by the *GMRGAL4* driver (*GMR>eIF6*), causes the formation of a reduced and rough adult eye (Fig 1A). We developed a new antibody specific for *Drosophila* eIF6 and we estimated its protein levels (Materials and Methods section) was about doubled compared to control (Fig 1B). The stereotypic structure of the wild-type eye was

severely disrupted with flattened ommatidia and bristles arranged in random patterns as shown by SEM analysis (Fig 1C). Semithin sections evidenced an aberrant morphology and arrangement of ommatidia (Fig 1D). These data show that increasing eIF6 levels in the fly eye cause a disruption of eye development.

Increased eIF6 levels delay physiological apoptosis

To understand the origin of the defects observed in *GMR>eIF6* adult eyes, we analyzed eye development in larvae, starting from the third instar, the stage at which the GMR driver starts to be expressed. We found that third instar imaginal discs with high levels of eIF6 showed no differences in terms of morphology, cell identity or developmental delay when compared to control (S2A-B Fig). Then, we analyzed pupal development. In *GMR>eIF6* retinae at 40h after puparium formation (APF) both neuronal and cone cells were present in the correct numbers. However, ommatidial morphology was altered (S2C Fig). A fundamental event controlling ommatidial morphology is the developmentally-controlled wave of Programmed Cell Death (PCD), sweeping the tissue from 25h to 42h APF (33). Thus, we analyzed by immunostaining the expression of *Drosophila* apoptotic effector caspase Dcp-1, as a marker of PCD, at 40h APF. Control retinae showed a clear presence of apoptotic cells. Remarkably, apoptotic cells were reduced in *GMR>eIF6* retinae (Fig 2A).

Dcp-1 positive cells, i.e. apoptotic cells, increased in *GMR>eIF6* retinae at 60h APF (Fig 2B). In summary, quantification of the number of Dcp-1 positive cells at 40h APF and 60h APF in *GMR>eIF6* revealed up to 75% reduction in the number of apoptotic cells at 40h APF, and an increase at 60h APF retinae (Fig 2C-D). A change in apoptosis dynamics was also visualized by TUNEL assay at 28h APF, the time at

which PCD starts in control retinae. Here, we observed the reduction of apoptotic nuclei in the *GMR>eIF6* retinae, while *GMRGAL4/+* retinae showed several (S2D Fig). In conclusion, eIF6 overexpression either blocks the early apoptotic program or delays it. We stained for the *Drosophila* β-catenin homologue Armadillo (Fig 3), which localizes to membranes of cells surrounding photoreceptors, providing an indication of ommatidial cell number. At 40h APF, control retinae presented the typical Armadillo staining. *GMR>eIF6* retinae showed the presence of extra-numerary cells around the ommatidial core (Fig 3A), indicating that interommatidial cells (IOCs) were not removed by PCD. By counting the number of cells in each ommatidium, we determined that *GMR>eIF6* retinae possess more than 13 cells, corresponding to approximately 30% more than that of a wild-type ommatidium (S3A Fig). Later in development, at 60h and at 72h APF, in *GMR>eIF6* retinae Armadillo was no longer detectable, while in wild-type retinae the pattern of Armadillo was maintained (Fig 3B and S3B Fig). These data indicate that delayed PCD in *GMR>eIF6* inappropriately removes most IOCs. We suggest that the first effect of eIF6 high levels is an early block of apoptosis that leads in turn to an aberrant developmental program.

Increased eIF6 expression in cone cells is sufficient to delay apoptosis

Cone cells and IOCs are known to be the main actors during physiological PCD (49). We overexpressed eIF6 under the control of the cone cell-specific driver, *spaGAL4*. We observed a milder phenotype compared to *GMR>eIF6* adult eyes (Fig 4A-B and S4A Fig). Importantly, eIF6 overexpression in cone cells (S4B Fig) caused reduced Dcp-1 staining in 40h APF retinae (Fig 4C), and evident apoptosis at 60h APF (Fig

4D), in line with what we observed in *GMR>eIF6* retinae. Thus, the expression of eIF6 in cone cells is sufficient to alter PCD and cause defects in eye development.

eIF6 expression reshapes the transcriptome, increases ribosome activity and represses ecdysone signalling

Next, we asked whether eIF6 was associated with a transcriptional rewiring that could account for the observed phenotypic effects. To this end, we performed a comprehensive gene expression analysis of *GMRGAL4/+* and *GMR>eIF6* genotypes at two distinct stages of eye development, larval eye imaginal discs and pupal retinae, by RNA-Seq (Fig 5). In *GMR>eIF6* samples at both developmental stages, we observed an upregulation of genes involved in ribosome biogenesis (Fig 5A, S1 File). GSAA analysis revealed also an increase in mRNAs of genes involved in rRNA processing (Fig 5C). Overall these data suggest that eIF6 is able to increase ribosomal gene expression.

Consistent with our phenotypic analysis of the eye, *GMR>eIF6* retinae displayed also variations in genes involved in eye development and in PCD (Fig 5A, D and S1 File). Notably, mRNAs encoding specialized eye enzymes, such as those of pigment biosynthetic pathways, were downregulated in *GMR>eIF6* samples (S1 File), preceding the altered adult eye morphology.

Finally, coordinated changes induced by eIF6 in eye imaginal discs surprisingly clustered into the ecdysone pathway, with a striking downregulation of many enzymes involved in 20-HydroxyEcdysone (20HE) biosynthesis (Fig 5 A-B). For instance, expression of *phm*, *sad* and *nvd* (S5 Fig) was virtually absent in *GMR>eIF6*

eye imaginal disc, while early (*rbp*) and late (*ptp52f*) responsive genes belonging to the hormone signalling cascade were downregulated (S1 File). In conclusion, our gene expression analysis of *GMR>eIF6* eye samples identifies a rewiring of transcription that is consistent with altered PCD, accompanied by upregulation of ribosomal genes and downregulation of the ecdysone biosynthetic pathway.

Increased eIF6 levels result in elevated translation

eIF6 binds free 60S *in vitro* and *in vivo* affecting translation (7). To assess whether increased transcription of genes related to ribosome biogenesis and rRNA processing observed in gene expression analysis experiments was accompanied by an effect on the translational machinery, we investigated changes in levels of free 60S subunits upon eIF6 overexpression. To this end, we performed the *in vitro* Ribosome Interaction Assay (iRIA) (44), able to measure quantitative binding of proteins to ribosomes. We found that the expression of eIF6 in *GMR>eIF6* larval eye discs led to a 25% reduction in free 60S sites when compared to control (Fig 6A). Next, we used a modified SUnSET assay (36), as a proxy of the translational rate. We measured translation in eye imaginal discs treated *ex vivo* with puromycin, which incorporates in nascent protein chains by ribosomes. Remarkably, *GMR>eIF6* eye discs incorporated almost twice the amount of puromycin, relative to control (Fig 6B-C). Taken together, high levels of eIF6 increase the free 60S pool *in vivo*, and increase puromycin incorporation, i.e. translation.

We next determined whether the increase of translation, altered morphology and apoptosis correlate with heightened eIF6 levels in other organs. Thus, we overexpressed eIF6 in the wing imaginal disc, using the *bxMS1096GAL4* driver

(*MS>eIF6*) (S6A Fig). Such manipulation led to complete disruption of the adult wing structure (Fig 6D). Moreover, we performed the SUnSET assay on wing imaginal discs, and, as in eye discs, we observed a two-fold increase in puromycin incorporation in *MS>eIF6* wing discs' respect to control (Fig 6E and S6B Fig). Finally, eIF6 overexpression in wing discs led to an increase of apoptotic cells in the dorsal portion of the disc (S6C Fig), as observed in 60h APF *GMR>eIF6* retinae. In conclusion, high levels of eIF6 lead not only to augmented expression of ribosomal genes, but also to augmented translational activity.

20HE administration rescues adult eye defects induced by increased eIF6 levels

Transcriptome analysis revealed a coordinated shut-down of the 20HE biosynthetic pathway raising the question whether 20HE administration could at least partly rescue the defects driven by eIF6 increased levels, and a rough eye phenotype characterized by aberrant PCD. To determine the hierarchy of events that eIF6 overexpression causes, we administrated 20HE by feeding *GMR>eIF6* third instar larvae and we evaluated the effect on eye development. Remarkably, *GMR>eIF6* larvae fed with 20HE showed eyes that were 20% larger than untreated controls (Fig 7A-B). We also assessed the levels of apoptosis at 40h APF. Notably, immunofluorescence staining for Dcp-1 showed the presence of apoptotic cells in 40h APF *GMR>eIF6* retinae treated with 20HE, while *GMR>eIF6* untreated retinae did not show any Dcp-1 positive cells (Fig 7C). Taken together, these data suggest that the apoptotic defect and eye roughness caused by eIF6 overexpression are at

least partly due to the inactivation of ecdysone signalling, that precedes deregulation of PCD.

eIF6 and translation antagonize ecdysone biosynthesis during development

Our findings indicate that increased eIF6 levels cause downregulation of mRNAs belonging to the ecdysone biosynthetic pathway, and the relative absence of its final product, the 20HE. To understand the physiological relevance of this phenomenon, we measured mRNAs levels of *eIF6* and *shd* at different stages of development (Fig 7). *Shd* encodes for the last enzyme of the 20HE biosynthesis and it is specifically expressed in ecdysone target tissues (50). Real-Time PCR evidenced the downregulation of *shd* in eye imaginal disc overexpressing eIF6 (Fig 7D). We then investigated the levels of *eIF6* and *shd* during development in wild-type tissues (Fig 7E-F). Interestingly, we found that eIF6 levels are regulated during development, and that *shd* levels drop when *eIF6* levels are high, both in embryos and first instar larvae (Fig 7E) or first and third instar larvae (Fig 7F). Importantly, 20HE levels drop at 40h APF retinae upon eIF6 overexpression (Fig 7G). Taken together, data suggest that physiological eIF6 levels are inversely correlated with 20HE production.

Taken that high levels of eIF6 lead to an increase in general translation, we decided to study the relationship between the translational rate and ecdysone production in a physiological context. We assessed levels of *shd* and *EcR* (as an index of the feed-forward loop induced by 20HE itself (51)) mRNA levels in S2 cells after treatment with rapamycin or insulin to inhibit or stimulate translation respectively (Fig 7H-J). After insulin treatment, we observed the downregulation of *shd* and *EcR* mRNA levels (Fig 7H). Conversely, after rapamycin treatment, we found an upregulation of

the two analyzed genes (Fig 7J). These data support a physiological model in which translation is a negative regulator of ecdysone metabolism.

DISCUSSION

Eukaryotic Initiation Factor 6 *eIF6* is an evolutionarily conserved gene encoding for a protein necessary for ribosome biogenesis and translation initiation (8, 9). However, in mammals, eIF6 expression differs among tissues, with high levels in embryos and in cycling cells and almost undetectable levels in post-mitotic cells (13). Developmental studies in mice demonstrated that null alleles for this initiation factor are incompatible with life (8), whereas eIF6 haploinsufficiency is linked to an impairment in G1/S cell cycle progression (8). In unicellular models, eIF6 mutations rescue the quasi-lethal phenotype due to loss of ribosome biogenesis factors such as SBDS (10). Taken together, these data highlight how eIF6 expression, despite its ubiquitous function, is strictly regulated. Indeed, we found that doubling levels of eIF6 during development disrupts eye morphology, increases translation and changes gene expression. Overall, our data demonstrate that eIF6 is a translation factor able to drive a complex transcriptional reshaping.

Mechanistically, eIF6 binds to the 60S in the intersubunit space, interacting with rpL23 and to the sarcin-loop (SRL) of rpL24 (52), thus generating a steric hindrance that prevents the formation of an intersubunit bridge (53). *In vitro*, eIF6 can repress translation (54). In mice, however, high levels of eIF6 are required for both tumor progression (16), and insulin-controlled translation (7, 8). In *Drosophila*, we found that the overexpression of eIF6 leads to a reduction of the free 60S pool in eye imaginal discs, consistent with eIF6 biochemical activity. Such reduction could imply

lower general translation, due to less availability of 60S subunits, as in the case of *Sbds* mutants (55). Conversely, 60S could be already engaged with 40S into active translating 80S, thus heightening general translation. We favour the latter hypothesis because, by a puromycin incorporation assay, we observe a two-fold increase in general translation, both in the developing eye and the wing. Intriguingly, the transcriptome signature associated with high levels of eIF6 revealed also an increase in mRNAs encoding for rRNA processing factors, suggesting that ribosome biogenesis is positively affected by eIF6. In conclusion, we surmise that *in vivo* eIF6 may act as a powerful stimulator of ribosome synthesis and translation.

The effects associated with increased translation driven by eIF6 are at least two, a change in the ecdysone pathway and a delay in apoptosis. We found a strong reduction of ecdysone biosynthesis pathway in the eye imaginal disc driven by eIF6. Importantly, 40h APF retinae evidence a reduction in hormone levels and 20HE administration leads to a partial rescue of the developmental defects driven by eIF6 increased activity. Thus, our data suggest that eIF6 is upstream of ecdysone regulation. It has been recently suggested how translation regulation and hormonal signalling are tightly interconnected in *Drosophila* (56) and, more generally, that translation is a controller of metabolism (57, 58). Our experiments unveil an inverse correlation between translational capability and ecdysone production. Concerning apoptosis we showed that eIF6 expression leads to an early block in Programmed Cell Death, as previously demonstrated by others in *X. laevis* (59). The developmental defects driven by increased eIF6 levels are consistent with two scenarios: excess eIF6 could delay developmental PCD. Alternatively, PCD could be repressed at the correct developmental time and apoptotic elimination of defective cells overexpressing eIF6 could be triggered later independently of developmental

signals. The fact that overexpression of eIF6 in wing discs, which are not subjected to a developmental wave of apoptosis, leads to cell death, supports the latter hypothesis.

The developmental changes due to eIF6-driven translation are dramatic and include lethality, as well as disruption of development. In the past, similar effects were observed by the expression of another rate-limiting factor in translational initiation, eIF4E (60). It is unknown whether the developmental defects driven by eIF4E overexpression also included the arrest of ecdysone biosynthetic pathway, or an apoptotic block. However, in mammalian models, eIF4E and eIF6 share the common property of being rate-limiting for tumor growth and translation in several contexts (61-67).

The signalling to eIF6 is different from signalling to eIF4E (68), but the effects of inhibition of eIF4F complex by rapamycin are similar to eIF6 inhibition (8, 69). This result may reflect the fact that both eIF6 and eIF4F converge on similar metabolic pathways like lipid synthesis (20, 57) In summary, our study demonstrates that overexpression of eIF6 in developing organs is sufficient to induce an increase in ribosome biogenesis and translation that correlates with complex transcriptional and metabolic changes leading to hormonal and apoptotic defects. It will be interesting to further dissect the relationship between epigenetic, metabolic, and transcriptional changes associated with heightened eIF6 levels. Furthermore, our model may also be useful for *in vivo* screenings of compounds that suppress the effect of eIF6 overexpression.

ACCESSION NUMBER

ArrayExpress ID will be provided upon acceptance for publication.

ACKNOWLEDGEMENTS

We thank William Brook (Alberta Children's Hospital, Calgary) for *UASeIF6* stocks and Manolis Fanto (King's College, London) for stocks and suggestions. We thank Valeria Berno for imaging help and Vera Giulia Volpi for semithin sections preparation. We thank Alan Warren (MRC, Cambridge) for useful suggestions. This work was supported by ERC TRANSLATE 338999 and FONDAZIONE CARIPLO to SB. PC is supported by Fondazione Umberto Veronesi.

REFERENCES

1. Hershey JW, Sonenberg N, Mathews MB. Principles of translational control: an overview. Cold Spring Harb Perspect Biol. 2012;4(12).
2. Kressler D, Hurt E, Bassler J. A Puzzle of Life: Crafting Ribosomal Subunits. Trends Biochem Sci. 2017;42(8):640-54.
3. Kressler D, Linder P, de La Cruz J. Protein trans-acting factors involved in ribosome biogenesis in Saccharomyces cerevisiae. Mol Cell Biol. 1999;19(12):7897-912.
4. Venema J, Tollervey D. Ribosome synthesis in Saccharomyces cerevisiae. Annu Rev Genet. 1999;33:261-311.
5. Warner JR, Vilardell J, Sohn JH. Economics of ribosome biosynthesis. Cold Spring Harb Symp Quant Biol. 2001;66:567-74.
6. Miluzio A, Beugnet A, Volta V, Biffo S. Eukaryotic initiation factor 6 mediates a continuum between 60S ribosome biogenesis and translation. EMBO Rep. 2009;10(5):459-65.
7. Brina D, Miluzio A, Ricciardi S, Biffo S. eIF6 anti-association activity is required for ribosome biogenesis, translational control and tumor progression. Biochim Biophys Acta. 2015;1849(7):830-5.
8. Gandin V, Miluzio A, Barbieri AM, Beugnet A, Kiyokawa H, Marchisio PC, et al. Eukaryotic initiation factor 6 is rate-limiting in translation, growth and transformation. Nature. 2008;455(7213):684-8.
9. Ceci M, Gaviraghi C, Gorrini C, Sala LA, Offenhauser N, Marchisio PC, et al. Release of eIF6 (p27BBP) from the 60S subunit allows 80S ribosome assembly. Nature. 2003;426(6966):579-84.
10. Menne TF, Goyenechea B, Sanchez-Puig N, Wong CC, Tonkin LM, Ancliff PJ, et al. The Shwachman-Bodian-Diamond syndrome protein mediates translational activation of ribosomes in yeast. Nat Genet. 2007;39(4):486-95.
11. Wong CC, Traynor D, Basse N, Kay RR, Warren AJ. Defective ribosome assembly in Shwachman-Diamond syndrome. Blood. 2011;118(16):4305-12.
12. Biffo S, Sanvito F, Costa S, Preve L, Pignatelli R, Spinardi L, et al. Isolation of a novel beta4 integrin-binding protein (p27(BBP)) highly expressed in epithelial cells. J Biol Chem. 1997;272(48):30314-21.
13. Donadini A, Giodini A, Sanvito F, Marchisio PC, Biffo S. The human ITGB4BP gene is constitutively expressed in vitro, but highly modulated in vivo. Gene. 2001;266(1-2):35-43.
14. Miluzio A, Oliveto S, Pesce E, Mutti L, Murer B, Grosso S, et al. Expression and activity of eIF6 trigger malignant pleural mesothelioma growth in vivo. Oncotarget. 2015;6(35):37471-85.
15. Sanvito F, Piatti S, Villa A, Bossi M, Lucchini G, Marchisio PC, et al. The beta4 integrin interactor p27(BBP/eIF6) is an essential nuclear matrix protein involved in 60S ribosomal subunit assembly. J Cell Biol. 1999;144(5):823-37.
16. Miluzio A, Beugnet A, Grosso S, Brina D, Mancino M, Campaner S, et al. Impairment of cytoplasmic eIF6 activity restricts lymphomagenesis and tumor progression without affecting normal growth. Cancer Cell. 2011;19(6):765-75.
17. Gatza ML, Silva GO, Parker JS, Fan C, Perou CM. An integrated genomics approach identifies drivers of proliferation in luminal-subtype human breast cancer. Nat Genet. 2014;46(10):1051-9.
18. Benelli D, Cialfi S, Pinzaglia M, Talora C, Londei P. The translation factor eIF6 is a Notch-dependent regulator of cell migration and invasion. PLoS One. 2012;7(2):e32047.
19. Pinzaglia M, Montaldo C, Polinari D, Simone M, La Teana A, Tripodi M, et al. EIF6 over-expression increases the motility and invasiveness of cancer cells by modulating the expression of a critical subset of membrane-bound proteins. BMC Cancer. 2015;15:131.
20. Brina D, Miluzio A, Ricciardi S, Clarke K, Davidsen PK, Viero G, et al. eIF6 coordinates insulin sensitivity and lipid metabolism by coupling translation to transcription. Nat Commun. 2015;6:8261.
21. Miluzio A, Ricciardi S, Manfrini N, Alfieri R, Oliveto S, Brina D, et al. Translational control by mTOR-independent routes: how eIF6 organizes metabolism. Biochem Soc Trans. 2016;44(6):1667-73.

22. Gilbert LI, Rybczynski R, Warren JT. Control and biochemical nature of the ecdysteroidogenic pathway. Annu Rev Entomol. 2002;47:883-916.
23. Yamanaka N, Rewitz KF, O'Connor MB. Ecdysone control of developmental transitions: lessons from Drosophila research. Annu Rev Entomol. 2013;58:497-516.
24. Champlin DT, Truman JW. Ecdysteroid control of cell proliferation during optic lobe neurogenesis in the moth Manduca sexta. Development. 1998;125(2):269-77.
25. Champlin DT, Truman JW. Ecdysteroids govern two phases of eye development during metamorphosis of the moth, Manduca sexta. Development. 1998;125(11):2009-18.
26. Herboso L, Oliveira MM, Talamillo A, Perez C, Gonzalez M, Martin D, et al. Ecdysone promotes growth of imaginal discs through the regulation of Thor in D. melanogaster. Sci Rep. 2015;5:12383.
27. Lee CY, Wendel DP, Reid P, Lam G, Thummel CS, Baehrecke EH. E93 directs steroid-triggered programmed cell death in Drosophila. Mol Cell. 2000;6(2):433-43.
28. Nicolson S, Denton D, Kumar S. Ecdysone-mediated programmed cell death in Drosophila. Int J Dev Biol. 2015;59(1-3):23-32.
29. Brand AH, Perrimon N. Targeted gene expression as a means of altering cell fates and generating dominant phenotypes. Development. 1993;118(2):401-15.
30. del Valle Rodriguez A, Didiano D, Desplan C. Power tools for gene expression and clonal analysis in Drosophila. Nat Methods. 2011;9(1):47-55.
31. Kumar JP. Building an ommatidium one cell at a time. Dev Dyn. 2012;241(1):136-49.
32. Cagan RL, Reh TA. Preface. Aspects of eye development: advances over the past twenty years. Curr Top Dev Biol. 2010;93:xi-xii.
33. Ready DF, Hanson TE, Benzer S. Development of the Drosophila retina, a neurocrystalline lattice. Dev Biol. 1976;53(2):217-40.
34. Ji Y, Shah S, Soanes K, Islam MN, Hoxter B, Biffo S, et al. Eukaryotic initiation factor 6 selectively regulates Wnt signaling and beta-catenin protein synthesis. Oncogene. 2008;27(6):755-62.
35. Harrison DA, Perrimon N. Simple and efficient generation of marked clones in Drosophila. Curr Biol. 1993;3(7):424-33.
36. Schmidt EK, Clavarino G, Ceppi M, Pierre P. SUnSET, a nonradioactive method to monitor protein synthesis. Nat Methods. 2009;6(4):275-7.
37. Bolger AM, Lohse M, Usadel B. Trimmomatic: a flexible trimmer for Illumina sequence data. Bioinformatics. 2014;30(15):2114-20.
38. Dobin A, Davis CA, Schlesinger F, Drenkow J, Zaleski C, Jha S, et al. STAR: ultrafast universal RNA-seq aligner. Bioinformatics. 2013;29(1):15-21.
39. Anders S, Pyl PT, Huber W. HTSeq--a Python framework to work with high-throughput sequencing data. Bioinformatics. 2015;31(2):166-9.
40. Love MI, Huber W, Anders S. Moderated estimation of fold change and dispersion for RNA-seq data with DESeq2. Genome Biol. 2014;15(12):550.
41. Xiong Q, Mukherjee S, Furey TS. GSAASeqSP: a toolset for gene set association analysis of RNA-Seq data. Sci Rep. 2014;4:6347.
42. Cordero J, Jassim O, Bao S, Cagan R. A role for wingless in an early pupal cell death event that contributes to patterning the Drosophila eye. Mech Dev. 2004;121(12):1523-30.
43. Montrasio S, Mlodzik M, Fanto M. A new allele uncovers the role of echinus in the control of ommatidial rotation in the Drosophila eye. Dev Dyn. 2007;236(10):2936-42.
44. Pesce E, Minici C, Babetaler J, Hurt E, Degano M, Calamita P, et al. Direct and high throughput (HT) interactions on the ribosomal surface by iRIA. Sci Rep. 2015;5:15401.
45. Harris MN, Ozpolat B, Abdi F, Gu S, Legler A, Mawuenyega KG, et al. Comparative proteomic analysis of all-trans-retinoic acid treatment reveals systematic posttranscriptional control mechanisms in acute promyelocytic leukemia. Blood. 2004;104(5):1314-23.

46. Martin B, Sanz R, Aragues R, Oliva B, Sierra A. Functional clustering of metastasis proteins describes plastic adaptation resources of breast-cancer cells to new microenvironments. J Proteome Res. 2008;7(8):3242-53.
47. Rosso P, Cortesina G, Sanvito F, Donadini A, Di Benedetto B, Biffo S, et al. Overexpression of p27BBP in head and neck carcinomas and their lymph node metastases. Head Neck. 2004;26(5):408-17.
48. Spradling AC, Stern D, Beaton A, Rhem EJ, Laverty T, Mozden N, et al. The Berkeley Drosophila Genome Project gene disruption project: Single P-element insertions mutating 25% of vital Drosophila genes. Genetics. 1999;153(1):135-77.
49. Rusconi JC, Hays R, Cagan RL. Programmed cell death and patterning in Drosophila. Cell Death Differ. 2000;7(11):1063-70.
50. Petryk A, Warren JT, Marques G, Jarcho MP, Gilbert LI, Kahler J, et al. Shade is the Drosophila P450 enzyme that mediates the hydroxylation of ecdysone to the steroid insect molting hormone 20-hydroxyecdysone. Proc Natl Acad Sci U S A. 2003;100(24):13773-8.
51. Niwa YS, Niwa R. Transcriptional regulation of insect steroid hormone biosynthesis and its role in controlling timing of molting and metamorphosis. Dev Growth Differ. 2016;58(1):94-105.
52. Klinge S, Voigts-Hoffmann F, Leibundgut M, Arpagaus S, Ban N. Crystal structure of the eukaryotic 60S ribosomal subunit in complex with initiation factor 6. Science. 2011;334(6058):941-8.
53. Weis F, Giudice E, Churcher M, Jin L, Hilcenko C, Wong CC, et al. Mechanism of eIF6 release from the nascent 60S ribosomal subunit. Nat Struct Mol Biol. 2015;22(11):914-9.
54. Russell DW, Spremulli LL. Mechanism of action of the wheat germ ribosome dissociation factor: interaction with the 60 S subunit. Arch Biochem Biophys. 1980;201(2):518-26.
55. Calamita P, Miluzio A, Russo A, Pesce E, Ricciardi S, Khanim F, et al. SBDS-Deficient Cells Have an Altered Homeostatic Equilibrium due to Translational Inefficiency Which Explains their Reduced Fitness and Provides a Logical Framework for Intervention. PLoS Genet. 2017;13(1):e1006552.
56. Rode S, Ohm H, Anhauser L, Wagner M, Rosing M, Deng X, et al. Differential Requirement for Translation Initiation Factor Pathways during Ecdysone-Dependent Neuronal Remodeling in Drosophila. Cell Rep. 2018;24(9):2287-99 e4.
57. Biffo S, Manfrini N, Ricciardi S. Crosstalks between translation and metabolism in cancer. Curr Opin Genet Dev. 2017;48:75-81.
58. Calamita P, Gatti G, Miluzio A, Scagliola A, Biffo S. Translating the Game: Ribosomes as Active Players. Front Genet. 2018;9:533.
59. De Marco N, Iannone L, Carotenuto R, Biffo S, Vitale A, Campanella C. p27(BBP)/eIF6 acts as an anti-apoptotic factor upstream of Bcl-2 during Xenopus laevis development. Cell Death Differ. 2010;17(2):360-72.
60. Hernandez G, Altmann M, Sierra JM, Urlaub H, Diez del Corral R, Schwartz P, et al. Functional analysis of seven genes encoding eight translation initiation factor 4E (eIF4E) isoforms in Drosophila. Mech Dev. 2005;122(4):529-43.
61. Carter JH, Deddens JA, Spaulding NI, Lucas D, Colligan BM, Lewis TG, et al. Phosphorylation of eIF4E serine 209 is associated with tumour progression and reduced survival in malignant melanoma. Br J Cancer. 2016;114(4):444-53.
62. De Benedetti A, Harris AL. eIF4E expression in tumors: its possible role in progression of malignancies. Int J Biochem Cell Biol. 1999;31(1):59-72.
63. Lazaris-Karatzas A, Montine KS, Sonenberg N. Malignant transformation by a eukaryotic initiation factor subunit that binds to mRNA 5' cap. Nature. 1990;345(6275):544-7.
64. Martinez-Saez E, Peg V, Ortega-Aznar A, Martinez-Ricarte F, Camacho J, Hernandez-Losa J, et al. peIF4E as an independent prognostic factor and a potential therapeutic target in diffuse infiltrating astrocytomas. Cancer Med. 2016;5(9):2501-12.

65. Oblinger JL, Burns SS, Akhmametyeva EM, Huang J, Pan L, Ren Y, et al. Components of the eIF4F complex are potential therapeutic targets for malignant peripheral nerve sheath tumors and vestibular schwannomas. Neuro Oncol. 2016;18(9):1265-77.
66. Robichaud N, Sonenberg N. Translational control and the cancer cell response to stress. Curr Opin Cell Biol. 2017;45:102-9.
67. Ruggero D. Translational control in cancer etiology. Cold Spring Harb Perspect Biol. 2013;5(2).
68. Loreni F, Mancino M, Biffo S. Translation factors and ribosomal proteins control tumor onset and progression: how? Oncogene. 2014;33(17):2145-56.
69. Beretta L, Gingras AC, Svitkin YV, Hall MN, Sonenberg N. Rapamycin blocks the phosphorylation of 4E-BP1 and inhibits cap-dependent initiation of translation. EMBO J. 1996;15(3):658-64.

Supporting Information captions:

S1. Strongly reduced or ubiquitously increased eIF6 levels are incompatible with life (A) *eIF6*^{k13214} mosaic analysis in wild type (Oregon R) wing margin and *eIF6* mutant clones (i and ii). Wild type control anterior wing margin (iii and iv). Wing margin clones induced in *Minute/eIF6*^{k13214} flies (v and vi) according to the crosses outlined in Materials and Methods. Mutant clones induced along the wing margin by using UAS-*Flp*; *C96*-GAL4; FRT*eIF6*^{k13214}/FRT *y+ pwn* flies (iv and vi). Arrows and arrowheads indicate *pwn eIF6*^{k13214} homozygous mutant and heterozygous *Minute* (*M/pwn eIF6*^{k13214}) tissues, respectively. Asterisks denote *y* twin cells and the "^" highlights heterozygous wild type bristles. **(B)** Ectopic embryonic *eIF6* phenotypes. Embryonic cuticle preparations in *TubGAL4/+* and *Tub>eIF6* evidencing that eIF6 increased levels is embryonic lethal.

S2. *GMR>eIF6* eye imaginal discs retain cell identity and morphology, opposite to *GMR>eIF6* retinae, which display altered morphology and PCD (A) *GMR>eIF6* and *GMRGAL4/+* eye imaginal discs stained for ELAV (neuronal cells marker) and Cut (cone cells marker) show that both neurons and cone cells preserve their identities upon eIF6 overexpression. **(B)** Counting ommatidial cluster rows in *GMR>eIF6* and *GMRGAL4/+* eye imaginal discs stained for ELAV shows that no developmental delay is associated with eIF6 overexpression. **(A-B)** Scale bar 50 µm. **(C)** Staining for ELAV, CUT and Chaoptin (intra-photoreceptor membranes marker) showing that both neurons and cone cells retain their identity. Noteworthy, neural and cone cells show an incorrect arrangement on the plane in association with increased eIF6 levels. Scale bar 10 µm. **(D)** TUNEL assay on early (28h APF) pupal stage retinae indicates that PCD is blocked at this developmental stage upon eIF6 overexpression. Scale bar 50 µm.

S3. Cell number is altered in *GMR>eIF6* retinae. (A) Comparison of cells number across two genotypes, *GMRGAL4/+* and *GMR>eIF6*, shows that there is an increase in *GMR>eIF6* with respect to control. 'Δ cells per ommatidium' refers to the number of cells gained or lost within an ommatidium (the number of cells in hexagon divided by 3). Results in the third column represent the mean ± SD, n=10. P-values were calculated using an unpaired two-tailed Student t-test. **(B)** Late-pupal stage (72h APF) retinae stained for Armadillo, the *Drosophila* β-catenin homologue, showing that when eIF6 is overexpressed cells around ommatidia are lost. Scale bar 10 µm.

S4. Increasing eIF6 levels only in cone cells results in aberrant morphology (A-B) Mid-pupal stage (40h APF) retinae of *spaGAL4/+* and *spa>eIF6* genotypes stained for ELAV and CUT confirm that neural and cone cell identity is retained, whereas cell arrangement is altered **(A)** upon eIF6 overexpression. **(B)** Mid-pupal stage (40h APF) retinae stained for eIF6 confirming that overexpression of eIF6 is restricted only to cone cells. **(A-B)** Scale bar 10 µm.

S5. RNASeq analysis reveals a strong downregulation of genes related to 20-HydroxyEcdysone biosynthesis. 20-HydroxyEcdysone biosynthetic pathway scheme. Genes involved in 20HE biosynthesis are strongly downregulated in *GMR>eIF6* eye imaginal disc, with respect to control. p-values from RNASeq analysis.

S6. eIF6 overexpression affects the wing. (A) Western Blot showing the levels of eIF6 expression in *MSGAL4/+* and *MS>eIF6* wing imaginal discs. Representative western blots from three independent experiments are shown to the left of each panel. **(B)** SUnSET assay performed using immunofluorescence experiment, indicating again a two-fold increase in general translation in *MS>eIF6* wing discs. For

each genotype, two magnifications are compared: 40x (scale bar, 63 µm) and, in the small squares, 252x (scale bar, 10 µm). **(C)** Apoptosis is increased in *MS>eIF6* wing imaginal disc. Wing discs stained for Dcp-1 and eIF6 in control flies (*MSGAL4/+*) and in *MS>eIF6*. In *MS>eIF6* there is a striking increase in apoptotic events, compared to the control. Scale bar 35 µm.

S1 File. Complete read counts of *GMR>eIF6* and *GMRGAL4/+* eye imaginal discs and pupal retinae List of all genes detected and tested for differential expression analysis in *GMR>eIF6* and *GMRGAL4/+* eye imaginal discs and pupal retinae. Gene quantification is calculated as normalized read counts.

FIGURE CAPTIONS

Fig 1. Increased eIF6 levels in the developing eye result in a rough eye phenotype (A) Representative stereomicroscope images of *GMRGAL4/+* and *GMR>eIF6* eyes, showing a rough eye phenotype. Scale bar 300 µm. **(B)** Western blot showing the levels of eIF6 expression in *GMRGAL4/+* and *GMR>eIF6* adult eyes. Representative western blots from three independent experiments are shown. Molecular weight markers (kDa) are shown to the left of each panel. The ratio was calculated with ImageJ software. The value corresponds to the intensity ratio between eIF6 and β-actin bands for each genotype. **(C)** Representative SEM images of *GMRGAL4/+* and *GMR>eIF6* adult eyes. eIF6 overexpressing eyes have an aberrant morphology, showing flattened ommatidia and randomly arranged bristles. Scale bar, respectively for 2400X, 5000X and 10000X magnifications are 10 µm, 5 µm and 2.5 µm **(D)** Representative tangential sections of *GMRGAL4/+* and

GMR>eIF6 adult eyes indicating that photoreceptors are still present in *GMR>eIF6* eyes, even if their arrangement is lost. Scale bar 10 µm.

Fig 2. The apoptotic wave is delayed when eIF6 levels are increased. (A) Mid-pupal stage retinae (40h APF) stained for the *Drosophila* caspase Dcp-1. *GMRGAL4/+* retinae show Dcp-1 positive cells, indicating that PCD is ongoing at this developmental stage. On the contrary, *GMR>eIF6* retinae do not show Dcp-1 positive cells, indicating a block in PCD. Scale bar 10 µm. **(B)** Late-pupal stage (60h APF) retinae stained for the *Drosophila* caspase Dcp-1. *GMRGAL4/+* retinae show a reduction of Dcp-1 positive cells, as expected (PCD already finished at this developmental stage). On the contrary, *GMR>eIF6* retinae, show Dcp-1 positive cells, indicating a delay in PCD associated with more eIF6 levels. Scale bar 10 µm. **(C-D)** Barplot showing the Dcp-1 positive cells counts average from four different areas (n=4) at 40h APF **(C)** and 60h APF **(D)** retinae with error bars indicating the SEM. P-values were calculated using an unpaired two-tailed Student t-test. Dcp-1 positive cells count indicates an overall delay and increases in PCD when eIF6 is increased during eye development.

Fig 3. Cell number is altered during the pupal stage in *GMR>eIF6* retinae. (A) Mid-pupal stage (40h APF) retinae stained for Armadillo, the *Drosophila* β-catenin homologue, showing that when eIF6 is increased there are extra-numerary cells (indicated as *) around each ommatidium. **(B)** Late-pupal stage (60h APF) retinae stained for Armadillo, showing the loss of all cells around ommatidia upon eIF6 overexpression. **(A-B)** Scale bar 10 µm.

Fig 4. A specific increase of eIF6 in cone cells results in a rough eye phenotype. (A-B) Overexpression of eIF6 in cone cells results in rough eye phenotype. **(A)** Representative stereomicroscope images of *spaGAL4/+* and *spa>eIF6* eyes showing a rough eye phenotype. Scale bar 300 μm **(B)** Representative tangential semithin sections of *spaGAL4/+* and *spa>eIF6* adult eyes showing disruption of the structure upon eIF6 overexpression in cone cells. Scale bar 10 μm. **(C)** Mid-pupal stage (40h APF) retinae of *spaGAL4/+* and *spa>eIF6* genotypes stained for Dcp-1 confirm the block in apoptosis already demonstrated in *GMR>eIF6* retinae. **(D)** Late-pupal stage (60h APF) retinae of *spaGAL4/+* and *spa>eIF6* genotypes stained for Dcp-1 confirming the delayed and increased apoptosis already observed in *GMR>eIF6* retinae. **(C-D)** Scale bar 10 μm.

Fig 5. eIF6 induces a reshaping of transcription, resulting in rRNA processing alteration and in a gene signature specific for the eye (A) Venn Diagram indicating genes differentially expressed in *GMR>eIF6* larval eye imaginal discs and *GMR>eIF6* retinae with respect to control (*GMRGAL4/+).* **(B)** The Ecdysone Biosynthetic Pathway is shut-down when eIF6 is upregulated. Heat Map representing absolute gene expression levels in *GMR>eIF6* and *GMRGAL4/+* eye imaginal disc samples for the subset of gene sets involved in Ecdysone Biosynthesis by Gene Ontology analysis. **(C)** Gene Set Association Analysis (GSAA) indicates a significant upregulation of the ribosomal machinery. Representative Enrichment Plots indicating a striking upregulation of genes involved in rRNA Processing (NAS: 2.24; FDR: 6,84E10-4) and Ribosome Biogenesis (NAS: 2.10; FDR: 0,013) in both *GMR>eIF6* eye imaginal discs and *GMR>eIF6* retinae with respect to their control (*GMRGAL4/+).* **(D)** mRNAs involved in Programmed Cell Death and in Eye

Differentiation are upregulated in *GMR>eIF6* retinae. Heat Map representing absolute gene expression levels in *GMR>eIF6* and *GMRGAL4/+* retinae samples for the subset of gene sets involved in Programmed Cell Death and Eye Differentiation by Gene Ontology Analysis.

Fig 6. Increased eIF6 levels in the developing eye result in reduced free 60S and increased translation. (A) iRIA assays showing that *eIF6* increased dosage reduce the number of free 60S subunits. Values represent the mean ± SEM from two replicates. Assays were repeated three times. Student's t-test was used to calculate p-values. **(B)** *In vitro* SUnSET assays showing that *eIF6* increased gene is associated with increased puromycin incorporation. Barplots represent the mean ± SEM from three replicates. Assays were repeated three times. Student's t-test was used to calculate p-values. Quantification of SUnSET assay was performed with ImageJ software. **(C)** Representative SUnSET assay performed using immunofluorescence experiments, indicating a two-fold increase in general translation when eIF6 levels are increased in eye imaginal discs. Scale bar 10 μm. **(D)** Adult wings *MS>eIF6* have a completely aberrant phenotype. Scale bar 200 μm. **(E)** *In vitro* SUnSET assays showing that *eIF6* increased gene is associated with 2-fold puromycin incorporation in wing discs. Barplots represent the mean ± SEM from three replicates. Assays were repeated three times. Student's t-test was used to calculate p-values. Quantification of SUnSET assay was performed with ImageJ software.

Fig 7. 20HE treatment rescues the rough eye phenotype due to high levels of eIF6, unveiling the role of translation in ecdysone biosynthesis regulation. (A-

C) 20HE treatment partially rescue the rough eye phenotype and the delay in apoptosis in 40h APF retinae **(A)** The barplot represents the average of n>8 independently collected samples with error bars indicating the SEM. P-values were calculated using an unpaired two-tailed Student t-test. The graph shows the *GMR>eIF6* adult fly eye size with or without treatment with 20HE. As indicated in the barplot, the fly eye size is partially rescued when the hormone is added to the fly food. **(B)** Representative stereomicroscope images of *GMR>eIF6* eyes treated (upper panel) or untreated (lower panel) with 20HE, showing a partial rescue of the eye size when 20HE has been added. Scale bar 100 µm **(C)** Immunofluorescence images showing that 20HE treatment (240 µg/mL in standard fly food) rescues the apoptotic delay observed in *GMR>eIF6* 40h APF retinae. Scale bar 50 µm **(D-F)** Real-time PCR analyses of the indicated genes showing an inverse correlation between *eIF6* and *shd* mRNA levels. The RNA level of each gene was calculated relative to *RpL32* expression as a reference gene. The barplot represents the average of at least three independent biological replicates with error bars indicating the SEM. p-values were calculated using an unpaired two-tailed Student t-test. **(D)** Real-time PCR analyses of the indicated genes in *GMRGAL4/+* and *GMR>eIF6* eye imaginal discs. Upon eIF6 overexpression, *GMR>eIF6* eye imaginal discs have less abundance of *shd* mRNA levels compared to *GMRGAL4/+* eye imaginal discs. **(E-F)** During development, *eIF6* and *shd* mRNA levels show an inverse correlation by comparing embryos with first instar larval RNA extracts **(E)** or by comparing first and third instar larval RNA extracts **(F)**. **(G)** Ecdysone titers in *GMR>eIF6 and GMRGAL4/+* eye imaginal discs and 40h APF retinae. 20HE levels decrease in 40h APF *GMR>eIF6* retinae respect to control retinae. **(H-J)** The ecdysone biosynthetic pathway genes *shd* and *EcR* are modulated upon translation modulation in S2 cells.

(H) Real time analysis evidences that upon inhibition of translation with rapamycin treatment (1 µM, 2 hours) the level of *shd* and *EcR* mRNA levels increase, contrary to the drop observed upon translation stimulation with insulin (1 µM, 12 hours). The RNA level of each gene was calculated relative to *RpL32* expression as a reference gene. The barplot represents the average of at least three independent biological replicates with error bars indicating the SEM. p-values were calculated using an upaired two-tailed Student t-test. **(J).** Representative western blot showing the decreased or increased rate of protein synthesis upon rapamycin or insulin treatment respectively with SUnSET method (36)

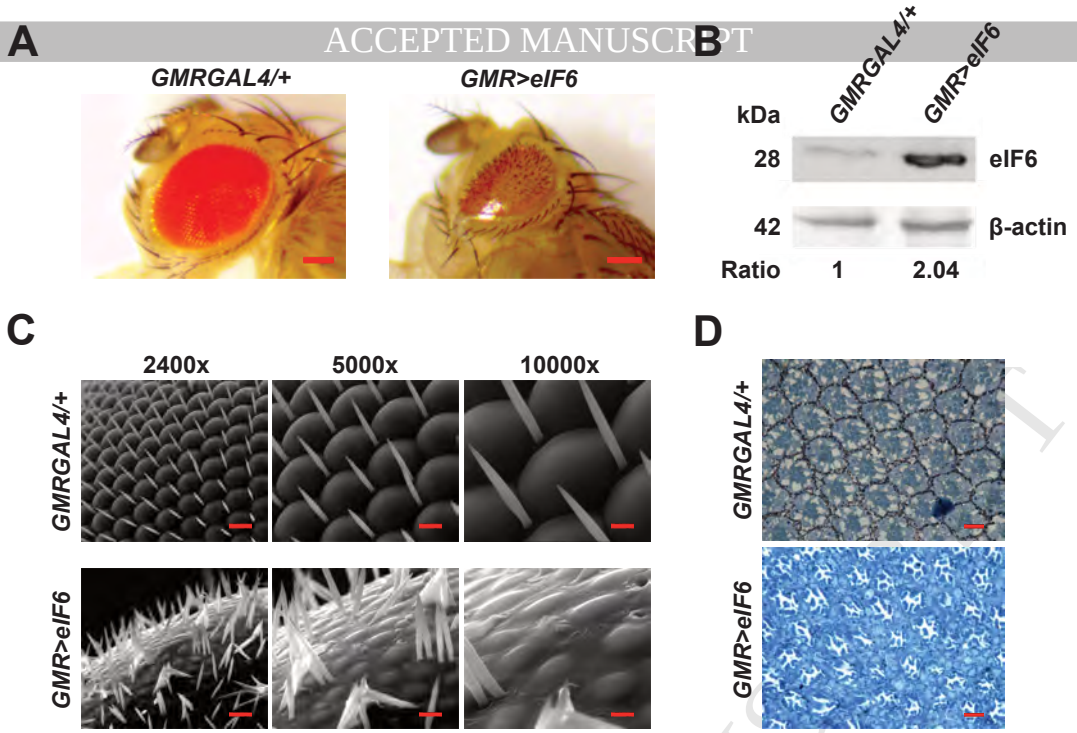

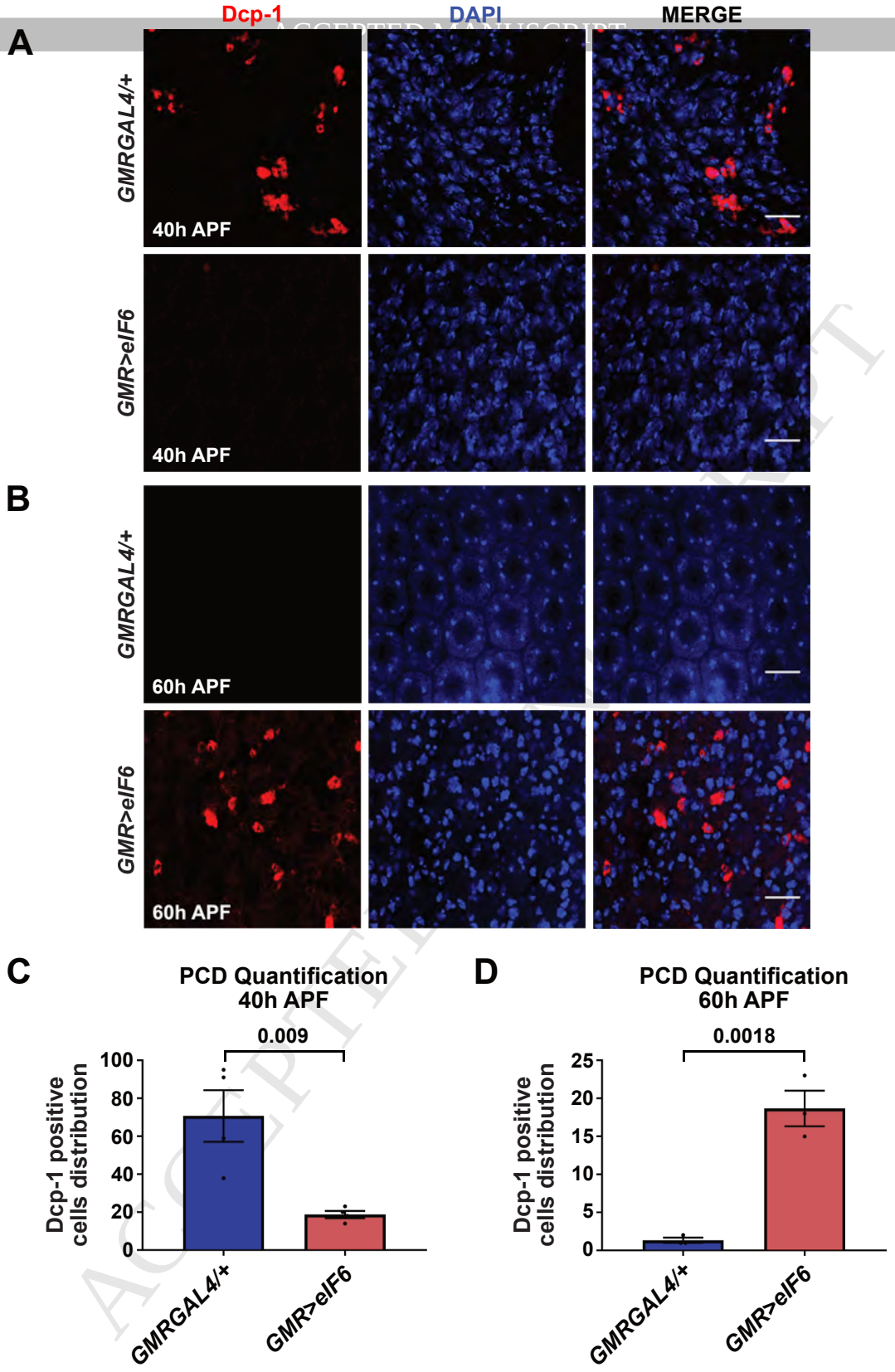

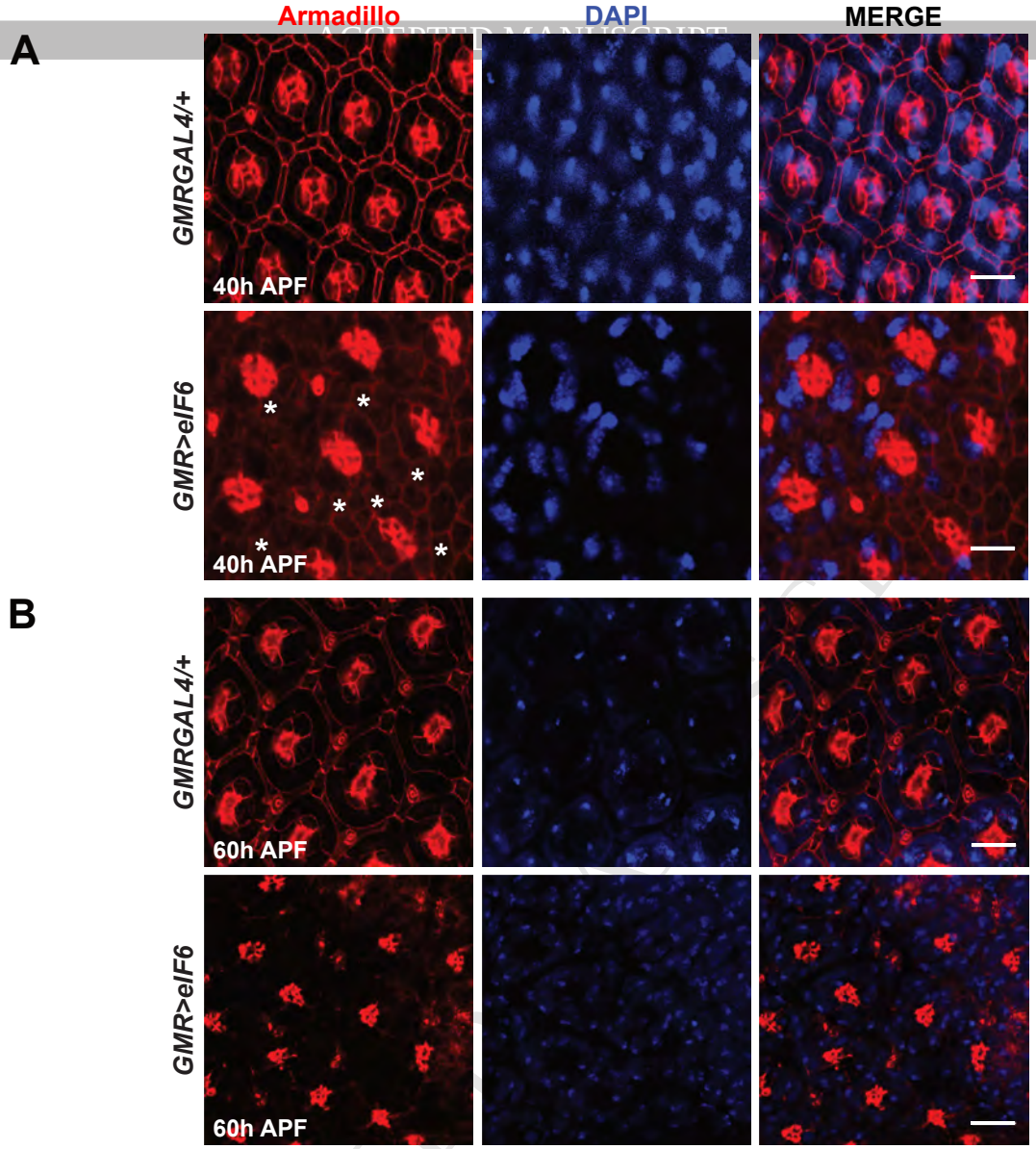

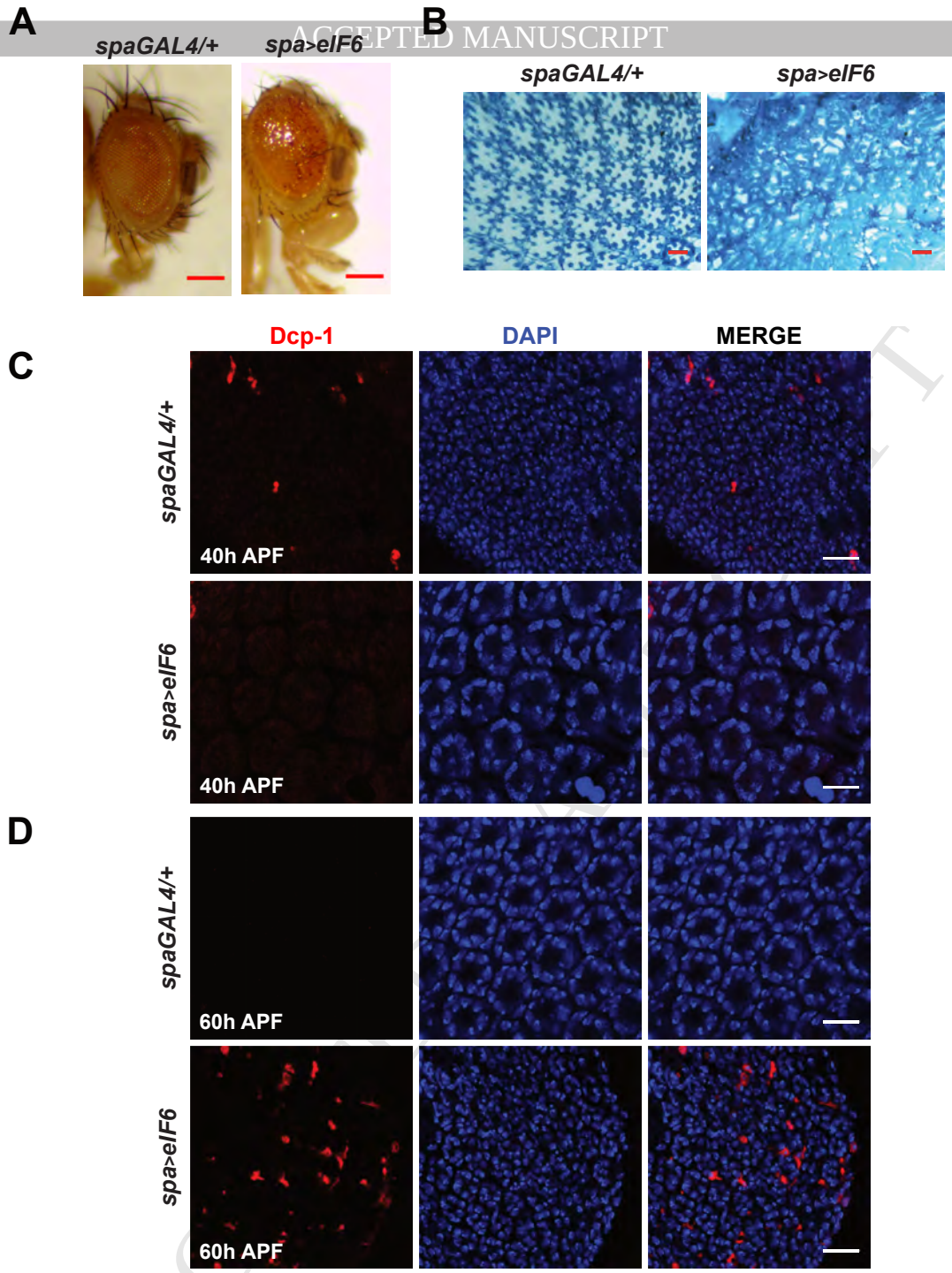

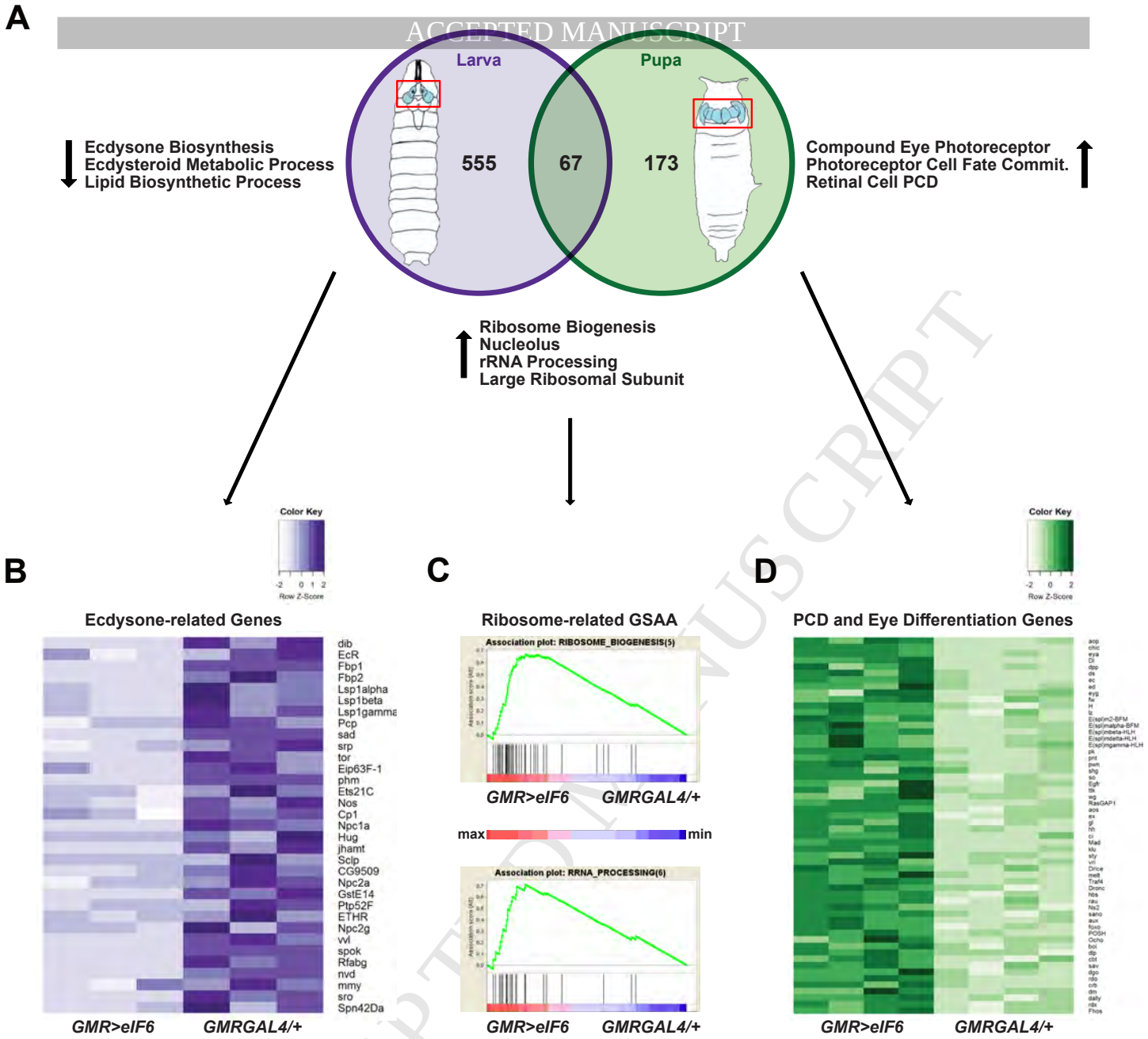

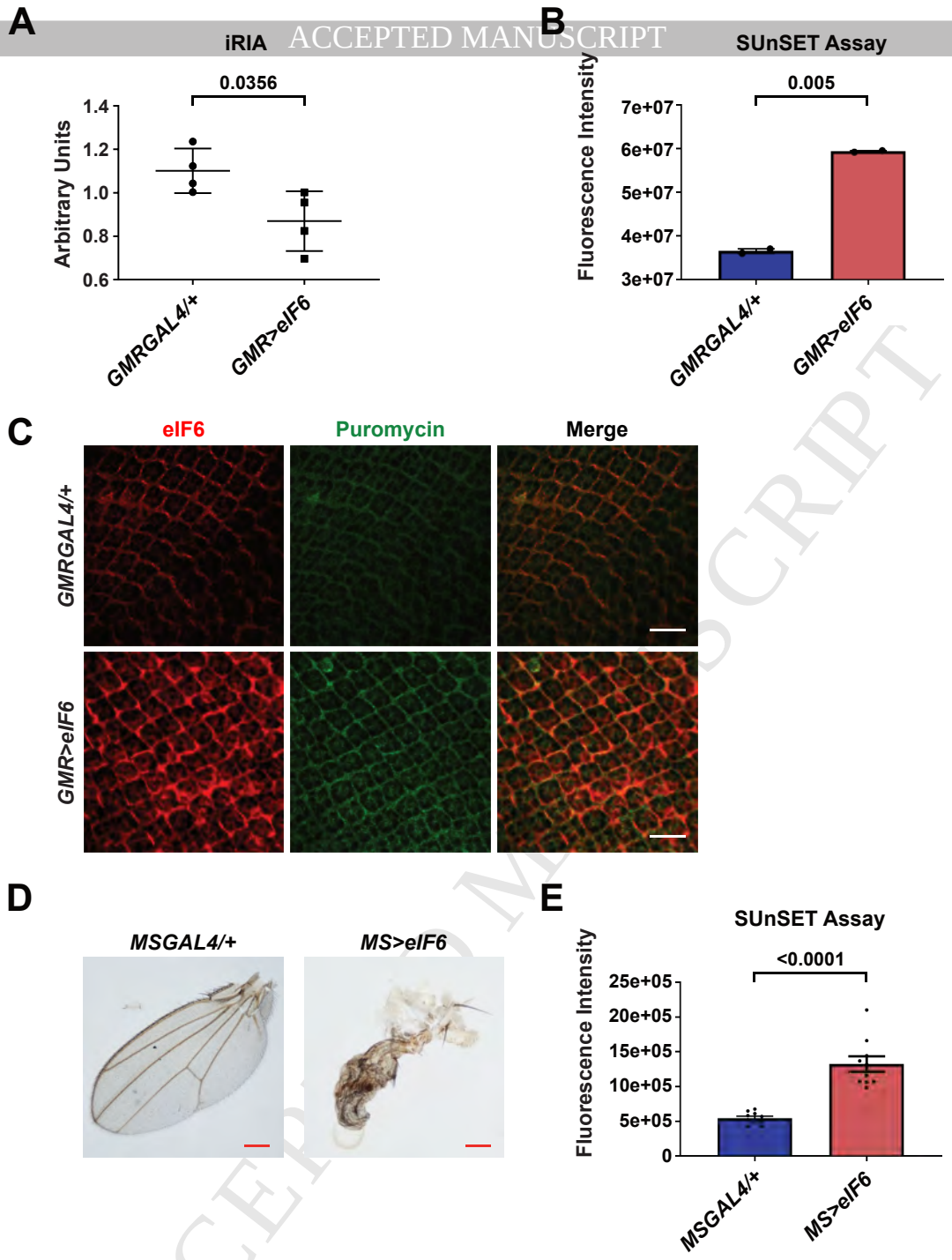

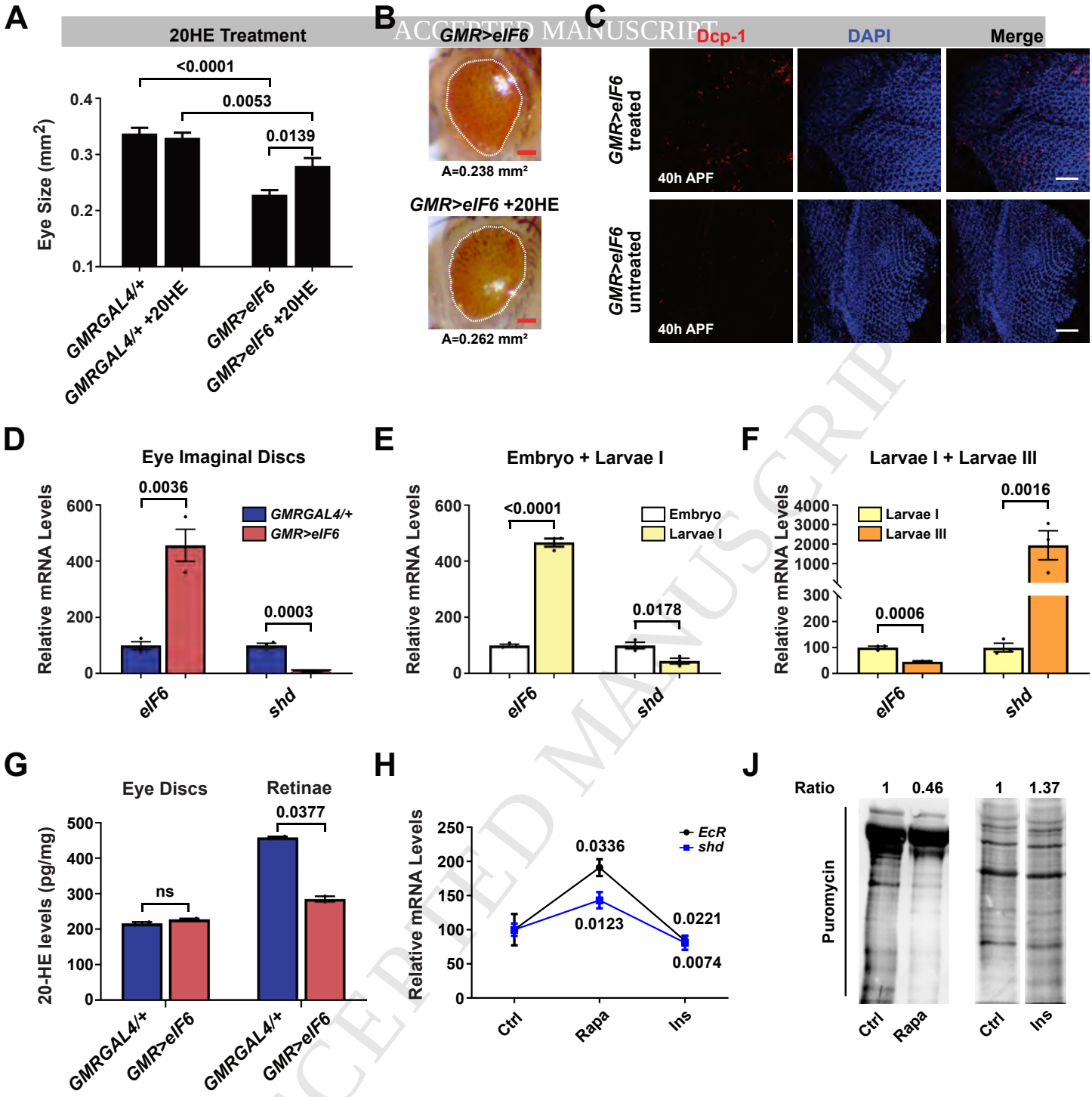

HIGHLIGHTS

- eIF6 high levels result in heightened general translation
- Ecdysone biosynthesis and general translational rate are inversely correlated
- Apoptosis is delayed by ecdysone biosynthesis shut-down during development

Key Resource Table

REAGENT or RESOURCE	SOURCE	IDENTIFIER
Antibodies		
Rabbit anti-eIF6	This study	N/A
Rabbit anti-β-actin	Cell Signaling Technology	RRID:AB_330288
Mouse anti-Puromycin (clone 12D10)	Millipore	RRID:AB_2566826
Rat anti-Elav	DHSB	RRID:AB_528218
Mouse anti-Cut	DSHB	RRID:AB_528186
Mouse anti-Armadillo	DSHB	RRID:AB_528089
Mouse anti-Chaoptin	DSHB	RRID:AB_528161
Rabbit anti-Dcp-1	Cell Signaling Technology	RRID:AB_2721060
Sheep anti-mouse IgG-HRP	GE Healthcare	RRID:AB_772210
Donkey anti-rabbit IgG-HRP	GE Healthcare	RRID:AB_772206
Goat anti-mouse IgG, Alexa Fluor 488	Life Technologies	RRID:AB_142924
Goat anti-rabbit IgG, Alexa Fluor 568	Life Technologies	RRID:AB_143157
Goat anti-rat IgG, Alexa Fluor 647	Life Technologies	RRID:AB_141778
Chemicals, Peptides, and Recombinant Proteins		
Rapamycin	Sigma	Cat#R8781
Insulin	Sigma	Cat#I0516
Puromycin	ThermoFisher Scientific	Cat#A1113803
Protease Inhibitors	Sigma	Cat#P8340
20-HydroxyEcdysone	Sigma	Cat#H5142
DAPI	Molecular Probes	Cat#D3571
Durcupan™ ACM	Sigma	Cat#44610-1EA
Critical Commercial Assays		
BCA Protein Assay Kit	Pierce	Cat#23227
In Situ Cell Death Detection Kit TMR Red	Roche	Cat#12156792910
SuperScript III First-Strand Synthesis SuperMix for qRT-PCR	Invitrogen	Cat#11752-050
SuperSignal™ West Pico PLUS Chemiluminescent Substrate	ThermoFisher Scientific	Cat#34577
mirVana™ miRNA Isolation Kit	Life Technologies	Cat#AM1560
DNA-free™ DNA Removal Kit	Life Technologies	Cat#AM1906
Qubit® RNA Assay Kit	Life Technologies	Cat#Q32852
TaqMan® Universal PCR Master Mix	Life Technologies	Cat#4304437
GoTaq® qPCR Master Mix	Promega	Cat#A6001
TruSeq RNA Library Prep Kit v2	Illumina	Cat#RS-122-2001
SBS Kit v3	Illumina	Cat#FC-401-3001
Enzyme Immunoassay Kit	Bertin Pharma	Cat#A05120.96
Deposited Data		

Accession number ID will be provided upon acceptance for publication	ArrayExpress	N/A
Experimental Models: Organisms/Strains		
D. melanogaster: *GMRGAL4/CTG*	A gift from Manolis Fanto (King's College, London)	N/A
D. melanogaster: *UAS-eIF6*	A gift from William J Brook (Alberta Children's Hospital, Calgary)	N/A
D. melanogaster: *y[1] w[*]; P{w[+mC]=tubP-GAL4}LL7/TM3, Sb[1] Ser[1]*	Bloomington Drosophila Stock center	BDSC: 5138
D. melanogaster: *P{w[+mC]=spa-GAL4.J}1, w[*]*	Bloomington Drosophila Stock center	BDSC: 26656
D. melanogaster: *y[1] w[*]; P{w[+m*]=GAL4}54C*	Bloomington Drosophila Stock center	BDSC: 27328
D. melanogaster: *w[1118]*	Bloomington Drosophila Stock center	BDSC: 3605
D. melanogaster: *w[1118] P{w[+mW.hs]=GawB}Bx[MS1096]*	Bloomington Drosophila Stock center	BDSC: 8860
Experimental Models: Cell Lines		
D. melanogaster: Schneider S2 cells	DGRC	RRID:CVCL_TZ72
Oligonucleotides		
Drosophila eIF6	Applied Biosystem	CAT#Dm01844498_g1
Drosophila RPL32	Applied Biosystem	CAT#Dm02151827_g1
Drosophila Shd	Metabion	F 5'-CGGATCGATATGCTAAGCTGT-3', R 5'-CGACGCACTCYCYYGTCG-3'
Drosophila RPL32	Metabion	F 5'-TCTCGCTCTTGTCGTGTCTG-3', R 5'-CCGATATCCTTCGCGTACTG-3'

Software and Algorithms		
R environment for statistical computing (version 3.3.1)	N/A	https://www.r-project.org/
FastQC (version 0.11.2)	Andrews, S. (2014)	http://www.bioinformatics.babraham.ac.uk/projects/fastqc
Trimmomatic (version 0.32)	Bolger, A. M. et al. (2014)	http://www.usadellab.org/cms/?page=trimmomatic
STAR software (version 2.4.1c)	Dobin, A. et al. (2013)	https://github.com/alexdobin/STAR
HTSeq-count (version 0.6.1)	Anders, S. et al. (2015)	https://pypi.org/project/HTSeq/
DESeq2 (version DESeq2_1.12.4)	Love, M.I. et al. (2014)	https://github.com/mikelove/DESeq2
topGO (version topGO_2.24.0)	Alexa, A. et al. (2016)	https://bioconductor.org/packages/release/bioc/html/topGO.html
GSAA (version 2.0)	Xiong, Q. et al. (2014)	http://gsaa.unc.edu/
Volocity (version 6.3)	Quorum Technologies	http://quorumtechnologies.com/index.php/2014-06-19-13-10-00/2014-06-19-13-14-30/image-analysis/2-uncategorised/110-volocity-downloads
Microsoft Excel	Microsoft	https://www.microsoft.com/
ImageJ	ImageJ	https://imagej.nih.gov/ij/
GraphPad 7	Prism	https://www.graphpad.com/scientific-software/prism/

Contact for Reagent and Resource Sharing

Further information and requests for reagents may be directed to, and will be fulfilled by the corresponding authors Piera Calamita (calamita@ingm.org) and Stefano Biffo (biffo@ingm.org).